ACS APPLIED ENERGY MATERIALS

UNIVERSITY OF EXETER

Subscriber access provided by the University of Exeter

Article

Enhanced Photoactivity and Hydrogen Generation of LaFeO Photocathode by Plasmonic Silver Nanoparticle Incorporation

Govinder Singh Pawar, Ameen Elikkottil, Sreeja Seetha, Srinivas Reddy, Bala Pesala, Asif Ali Tahir, and Tapas K. Mallick

ACS Appl. Energy Mater., **Just Accepted Manuscript** • DOI: 10.1021/acsaem.8b00628 • Publication Date (Web): 15 Jun 2018

ACS Publications

is published by the American Chemical Society. 1155 Sixteenth Street N.W., Washington, DC 20036

Enhanced Photoactivity and Hydrogen Generation of $LaFeO_3$ Photocathode by Plasmonic Silver Nanoparticle Incorporation

Govinder Singh Pawar, [1] Ameen Elikkottil, [2, 3] Sreeja Seetha, [2,4] Srinivas Reddy, [5] Bala Pesala*, [2, 3] Asif Ali Tahir*, [1] Tapas Kumar Mallick.[1]

[1] Environment and Sustainability Institute, University of Exeter, Penryn, Cornwall, TR10 9FE, United Kingdom

[2]Academy of Scientific and Innovative Research (AcSIR), Taramani, Chennai - 600113, India

[3] CSIR – Structural Engineering Research Centre (CSIR-SERC), Taramani, Chennai – 600113, India

[4] CSIR - Central Electronics Engineering Research Institute (CSIR-CEERI), CSIR Madras Complex, Taramani, Chennai – 600113, India

[5]Indian Institute of Technology, Madras, Chennai – 600036, India

Keywords: Hydrogen evolution, Photoelectrochemical (PEC), water splitting, surface plasmon resonance (SPR), Ag nanoparticles, $LaFeO_3$, photocathode, Finite Difference Time Domain (FDTD).

Abstract

A plasmonic $LaFeO_3$-Ag (LFO-Ag) photocathode was synthesised by incorporating Ag nanoparticles to excite surface plasmon resonances (SPR) for enhanced light harvesting to drive photoelectrochemical (PEC) hydrogen evolution. The Ag nanoparticles were modelled using finite difference time domain (FDTD) simulations and the results show an optimal dimension of 50-80 nm for SPR enhancement. Nanostructured LFO films were prepared by a novel and inexpensive spray pyrolysis method and the Ag nanoparticles were dispersed uniformly on to the films by simple spin coating method. The LFO-Ag photocathode exhibited strong light absorption capability and high current density, twice that than of its untreated counterpart. This subsequently led to enhanced PEC hydrogen evolution, doubling the volume of hydrogen generated compared to untreated LFO. The enhancement is ascribed to the strong SPR effect and the synergy between the Ag nanoparticles and nanostructured LFO photocathode.

Introduction

With the emergence of developing countries growing economy and population, fossil fuels will not be able to sustain the global demand for energy as they are being exhausted at an alarming rate.[1,2] Also, the emergence of these developing countries and their new spending capacity is increasing global CO_2 emissions at a frightening rate.[3] Hydrogen is a promising alternative fuel capable of replacing fossil fuels as a primary source of energy as it has high energy density (140 MJ kg^{-1}), far exceeding that of fossil fuels, zero carbon emission and the only by-product from combustion is water.[4] Current methods of hydrogen production in industry are as follows: hydrocarbon reforming, hydrogen from biomass and electrolysis. These methods however have some disadvantages. In hydrocarbon reforming process; carbon monoxide is released as a by-product. Biomass gasification suffers from low thermal

efficiency and any addition of steam or oxygen results in steam reforming leading to the production of carbon monoxide. Electrolysis of water requires an electric current, which is provided by fossil fuels from the electrical grid, to break down water into its constituents (O_2 and H_2).[5]

Photoelectrochemical (PEC) water splitting is widely recognized as one of the most promising approach for large scale solar energy conversion to storable fuels (hydrogen).[6–9] The process for PEC water splitting involves the light energy being absorbed by a semiconductor material to generate electron-hole pairs, and the photoexcited electrons/holes are driven by the space-charge field to the semiconductor/electrolyte solution interface where they reduce/oxidize water.[10,11] P-type semiconductors are used for Hydrogen Evolution Reaction (HER), as its conduction band is located more negative than H_2O/ H_2 potential.[11] Cu_2O[12], NiO[13] and $CaFe_2O_4$[14] are some metal oxide based p-type semiconductor materials used for HER. These materials show good potential for photocatalytic activity for hydrogen evolution; however, there are a few drawbacks for these materials. Cu_2O has one of the highest current densities (10 mA/cm^2) of metal oxide semiconductor; but has very poor stability as the film deteriorates in few minutes under PEC conditions.[15] NiO is a highly stable material under PEC conditions, however it exhibits poor photon harvesting performance due to its large band gap (3.45 eV) yielding lower amount of hydrogen.[13] $CaFe_2O_4$ is a promising material as it has a narrow band gap (1.9 eV) and band edges straddling the redox potential of water. However, the high annealing temperatures (1100 - 1200^{o}C) required to synthesise the material makes it economically unviable.[14]

$LaFeO_3$ (LFO) photocathode has recently been fabricated by a novel, cost effective and scalable spray pyrolysis method and has demonstrated hydrogen generation, from solar water splitting, without any applied external bias[16]. It has a band gap of 2.4 eV allowing it to access the visible region of the solar spectrum. Its band edges straddle the redox potential of water, with its conduction band -1.11 V above the reduction potential of hydrogen. It also displays high stability even after 21 hours of chronoamperometric test; the film is still photoactive and shows no visible degradation under the scanning electron microscope (SEM). On the other hand, its photocurrent is relatively low when compared to other metal oxide semiconductors, for example Cu_2O, due to its low light absorption properties.[16] In the pursuit to improve light absorption to increase the hydrogen generation, an attempt has been made to increase the film thickness to enhance light absorption. However, charge recombination problem is encountered resulting in decreased photocurrent.

Surface Plasmon Resonance (SPR) has been considered as one of the best strategy to improve light harvesting capabilities of semiconductor materials.[17,18] Noble metals (e.g. gold[19–22] and silver[18,23]) have the potential of enhancing optical absorption and scattering by excitation of Surface Plasmon Resonance (SPR), thus improving light harvesting capabilities. Light-driven oscillations of conduction electrons cause oscillating dipoles and the right wavelengths excite strong SPR in metallic nanoparticles.[24] SPR in smaller nanoparticles results in higher surface electro-magnetic fields and hence higher scattering cross-section, much larger than geometric cross-section[25]. The enhanced electromagnetic field is dependent upon the wavelength of incident light, shape, size and aggregation state of the nanoparticles.[26] There are three mechanisms of plasmon-enhanced solar energy conversion: 1) light scattering/ trapping, 2) hot electron injection and 3) plasmon-induced resonance energy transfer (PIRET).[27,28] When

plasmonic metal nanoparticles are integrated with a semiconductor material, the incident light can be effectively scattered by the metal nanoparticles. Due to this scattering effect, enhanced light absorption and charge separation occur in the active semiconductor material. In hot electron injection, non-radiative dissipation of plasmon energy is capable of generating hot carriers via Landau damping. The hot electrons, which have energy higher than the Schottky barrier at the metal/ semiconductor interface, can be directly injected into the conduction band of the semiconductor. To maximise the hot electron injection effect, it is essential to keep close contact between metal and semiconductor. In the PIRET mechanism, the excited plasmon in a metal is able to generate a strong dipole. The plasmonic energy in the metal can be non-radiatively transferred to the semiconductor via the dipole-dipole interaction in the near field, generating electron/ hole pairs in the semiconductor material. PIRET is strongly dependent on two factors: 1) distance between the energy donor (metal) and energy acceptor (semiconductor), and 2) the spectral overlap between plasmonic resonance band and the semiconductor's absorption band. Therefore, plasmonic nanoparticles can be used as photosensitizers for semiconductors to significantly extend the light absorption spectral range. Silver (Ag) is of particular interest of the noble metals due to its lower cost (compared to gold) and controllable size. Enhanced optical absorption and enhanced photocurrent by applying silver nanoparticles (Ag nanoparticles), giving rise to surface plasmons, have been applied to silicon solar cells[29–32],dye-sensitized solar cells[17,26,33–36] and for hydrogen production from water splitting.[18,23] Along with plasmonic nanoparticles, quantum dots can also help improve charge carrier dynamics.[37]

Here, we report an approach towards enhanced photocurrent and hydrogen evolution capabilities of LFO photocathode, by incorporating Ag nanoparticles to provide a plasmonic enhanced LFO-Ag photocathode nanocomposite. To the best of our knowledge, this is the first time LFO-Ag photocathode has been fabricated to show enhanced photoactivity and hydrogen yield. Finite Difference Time Domain (FDTD) simulations are employed to simulate the SPR resonances of Ag nano particles. The FDTD simulations show that the Ag nanoparticles with diameters in the range of 50 - 80 nm demonstrate strong SPR effect suitable for incorporation with $LaFeO_3$ photocathodes. Experimentally, these nanoparticles show enhanced light extraction capabilities. This in turn gives rise to an increased photocurrent and hydrogen yield, where it more than doubles when Ag nanoparticles are incorporated in to the $LaFeO_3$ films.

Methods

FDTD 3D Simulations

Finite Difference Time Domain (FDTD) simulation tool from Lumerical (Lumerical FDTD v.8.6.2 (2013), Lumerical Solutions, Inc.) is used to study the spectral response of silver nanoparticles (Ag nanoparticles) with varying particle size. Ag parameters from Palik[38] material database are chosen for carrying out the simulations. Total Field Scattering Field (TFSF) light source (300 nm-700 nm) is used for the simulations with the surrounding environment refractive index of 1.335 (refractive index of 0.1 M NaOH solution). The

simulation region mesh size is 0.5 nm and Perfectly Matched Layer (PML) boundary conditions are applied to all the boundaries. A uniform mesh of 0.5 nm used in all the three directions. The diameter of Ag nanospheres is varied from 20 nm to 100 nm in steps of 10 nm. The extinction, absorption and scattering spectra are obtained from the simulations. Based on these spectra, the electrical field (|**E**|) distribution of Ag nanoparticles of 70 nm diameter at different wavelengths of incident light is also studied.

Preparation of $LaFeO_3$-Ag Photocathode

The $LaFeO_3$ photocathode was fabricated using spray pyrolysis method, where full details of the experimental procedure can be found in our previous work.[16] In brief, Iron (III) nitrate nonhydrate (1 mmol) was dissolved in 20 ml methanol and 20 ml 30% solution of NH_3 in water is added to generate precipitate of iron hydroxide. The precipitate is collected and washed two times with de-ionized water. The precipitate is dissolved in 0.1 ml Trifluoroacetic acid in 25 ml methanol and Lanthanum (III) iso-propoxide (1 mmol) was added and stirred until it completely dissolved. The solution was then sprayed onto clean fluorine doped tin oxide (FTO) glass substrate at 150 ^{o}C. The films were then further annealed at 550^{o}C for 3 hours in air. The silver nanoparticles (from Nanoshel) with 99.9% purity and size distribution ranging from 50-80 nm were incorporated into the $LaFeO_3$ films by spin coating method. The silver nano powder (0.77 mmol) is placed into a vial containing acetone. Subsequently, it was ultrasonicated for 2 hours to break down large particles and reduce the agglomeration for obtaining a homogeneous suspension of Ag nanoparticles in acetone. The concentrated Ag NP suspension was serially diluted to obtain concentrations of 0.37 mmol, 0.19 mmol and 0.10 mmol for photocathode performance evaluation. In addition to this, a higher concentration of 1.5 mmol solution was also prepared. A strip of Kapton tape was pasted on to FTO glass for electrical contact. Five different electrodes were prepared with these Ag nanoparticles solutions of various dilutions by spin coating at an rpm of 500 rpm for 30 seconds. These electrodes were then annealed at a low temperature of 50^{o}C for 15 minutes. This ensures the evaporation of acetone and enhances the binding of Ag nanoparticles to the film without their oxidation.

Instrument Details

Material Characterization

The material phase composition was determined using a Bruker D8 Advance X-Ray Diffractometer (XRD) (Cu Kα irradiation, 40 kV/ 40 mA, 0.02 ^{o}2θ step and a scan time of 3 seconds per step) in the range of 20-70^{o} 2θ. The morphology and composition of the thin film was characterized using a high resolution Scanning Electron Microscope (SEM, HITACHI S3200N) coupled with an Energy Dispersive Spectroscopy (EDS, Oxford instrument elemental analysis). Diffuse reflectance spectra were acquired using a spectrophotometer (PerkinElmer lambda 1050 with 150 mm integrated InGaAs sphere).

Electrochemical Characterization

All electrochemical experiments were carried out in a standard 3 electrode system, composed of a working electrode, Pt wire as counter electrode and a reference electrode of Ag/AgCl in

saturated KCl. The data collection was carried out using potentiostat (Metrohm Autolab PGSTAT302N). The working electrode potential versus the Ag/AgCl reference electrode used in all experiments was converted into the Reversible Hydrogen Electrode (RHE) using equation: $V_{RHE} = V_{Ag/AgCl} + 0.197\ V + 0.059\ V * pH$.

The photoelectrochemical (PEC) performance of $LaFeO_3$ photocathode was measured in 0.1 M NaOH aqueous solution (pH 13), where no sacrificial agents were used, under light illumination using a 300 W ozone free Xenon lamp equipped with an AM 1.5 filter (Newport 66902). A one sun illumination (100 mW/cm^2) is used. A Linear Sweep Voltammetry (LSV) scan in the positive to negative direction between the ranges of +0.35 V to -0.35 V is used for photocurrent measurements.

Chronoamperometric (CA) measurements of $LaFeO_3$-Ag was conducted over a period of 24 hours under a continuous 1 sun illumination. This was carried out in 0.1 M NaOH (pH 13) aqueous solution with no sacrificial agents, in a standard 3 electrode system in ambient atmosphere and temperature. A constant current of 0 V was maintained over the measurement period.

Hydrogen Evolution Measurements

Gas Chromatography (GC) measurements were carried out using a manual injection GC system (PerkinElmer Clarus 580) using a molecular sieve (PerkinElmer) and a Pulsed Discharge Detector (PDD) with an argon flow of 28 ml/min. A custom-made glass reactor vessel with an attached fused silica viewport containing 0.1 M NaOH (pH 13) with a dead space of 100 ml was purged with argon for 2 hours with gentle heating and stirring to remove atmospheric air from the system. No sacrificial agents were used. The sealed vessel contained the working $LaFeO_3$ electrode connected to a Pt mesh by a single outer wire and was subjected to light illumination for the water splitting reaction. GC measurements were carried at an interval of 1 hour.

Results and Discussion

FDTD Simulations: Extinction, Absorption and Scattering

Finite Difference Time Domain (FDTD) analysis using Lumerical software is used for the optimization of the nanoparticle, it is a numerical technique used for nanophotonic modelling to obtain an approximate solution to Maxwell's equations (electric and magnetic fields).

Fig. 1(a) to 1(f) show the extinction, absorption and scattering cross-sections of Ag nanoparticles with increasing diameter. The results show that both absorption and scattering cross-section increases with increase in diameter of Ag nanoparticles and the nanoparticles of diameters greater than 50 nm show a greater scattering component compared to absorption. This trend can be explained by noting that the absorption and scattering cross-sections are proportional to the cube and sixth power of diameter of nanoparticle respectively[39] and hence scattering dominates in larger nanoparticles. As the diameter of nanoparticles increase, the SPR peak broadens and experiences a red shift[40]. Red shift of the SPR peak is due to the weakening of the restoring force with increasing size of the nanoparticle[41]. A secondary peak becomes visible at lower wavelengths in addition to the primary peak for diameters greater

than 80 nm (Fig. 1(d)). Quadrupole resonances cause these secondary peaks which has a different electron oscillation pattern.[42–44] Though scattering increases with size, for our application, it is not recommended to use nanoparticles of sizes > 90 nm as these will have lower surface area to volume ratio and they tend to form larger aggregates. Hence, normalized scattering cross-section (scattering cross-section normalized to nanoparticle geometric cross-sectional area[25]) is calculated for Ag nanoparticles of diameter 40 nm to 80 nm with a step of 10 nm. Fig. 1(f) shows that initially, as the size of the Ag NP increases the normalized scattering cross-section increases, reaches a maximum value and then slightly decreases. Results show that for nanoparticle of size 70 nm, the best performing nanoparticle for light scattering, normalized scattering cross-section reaches 6.4 and in the diameter range of 50 – 80 nm its greater than 5. Moreover, for these NP dimensions, the peaks appear in the wavelength range of 421 – 447 nm (2.77 – 2.94 eV) which is higher than the bandgap of LFO (2.4 eV)[16] and for 70 nm diameter, the peak appears at 439.5 nm corresponding to an energy of 2.82 eV.

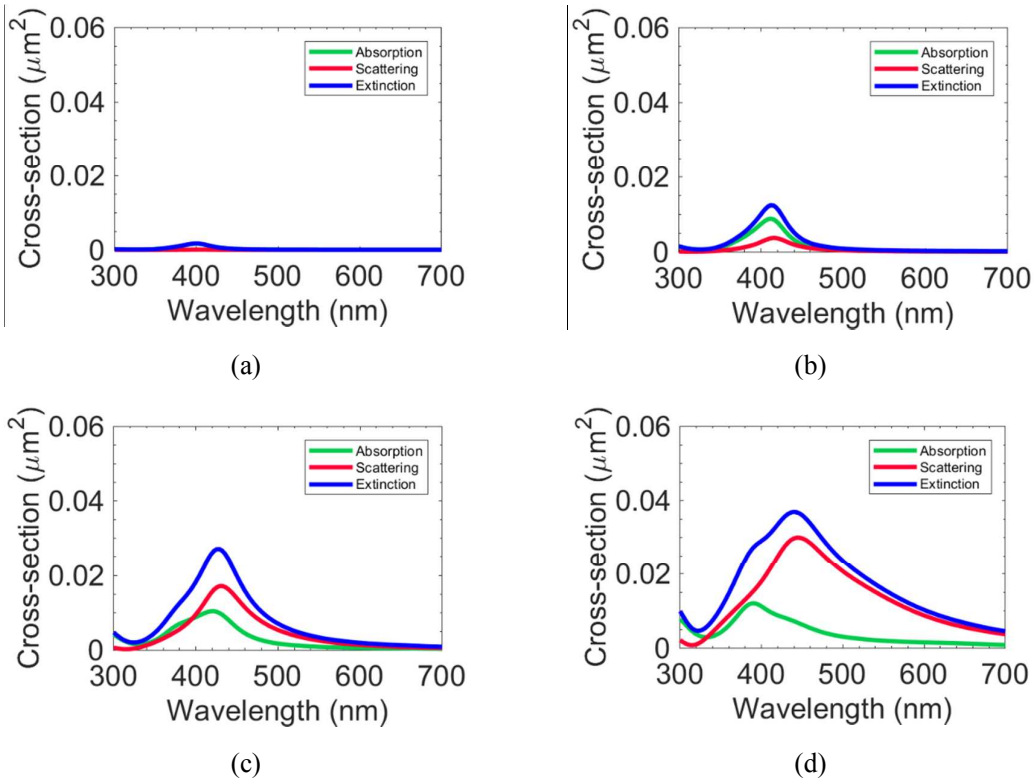

(a) (b)

(c) (d)

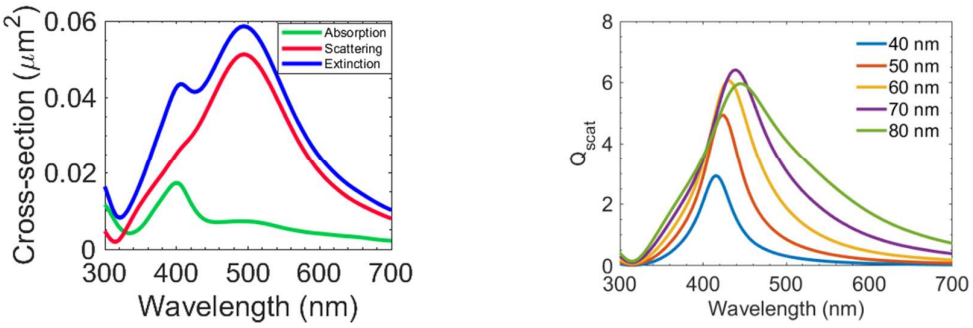

(e) (f)

Figure 1. Extinction, absorption and scattering cross-sections of Ag nanoparticles of diameters (a) 20 nm (b) 40 nm (c) 60 nm (d) 80 nm (e) 100 nm (f) normalized scattering cross-sections of Ag nanoparticles for diameters of 40-80 nm.

FDTD Simulations: Electric Field Profile of Ag NP of 70 nm at ON and OFF Resonances

The optimized size of the Ag nanoparticles is in the range of 50-80 nm and hence a NP of diameter 70 nm is chosen for studying its electric field profile at different wavelengths of incident light, as it is the best performing NP size. The refractive index of the surrounding medium was set as 1.335 (0.1 M NaOH in water). For 70 nm particle, the SPR peak is at 439.5 nm. Fig. 2(a) and 2(b) shows the distribution of the magnitude of electric field (|**E**|) at OFF (λ=300 nm) resonance and ON resonance (λ=439.5 nm). The results clearly show a field enhancement of more than 7 near the surface of Ag NP at surface plasmon resonance wavelength which would result in efficient light harvesting suitable for plasmonic enhancement of photo-catalytic water splitting.

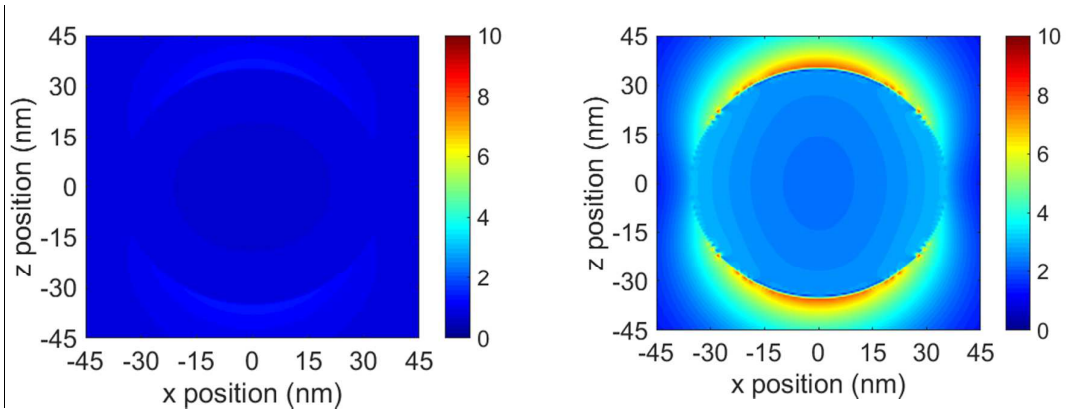

(a) (b)

Figure 2. Magnitude of electric field for Ag NP of diameter 70 nm at (a) **λ** = 300 nm (OFF Resonance) (b) **λ**= 439.5 nm (ON Resonance).

Performance and Characterization of LFO-Ag Photocathode

The LFO films were prepared by spraying the precursor solution at 150^{o}C and then post-annealed at 550^{o}C to obtain single phase crystalline material. The optimized size from theoretical modelling is 50-80 nm and similar range is used in fabrication of photo electrode. Ag nanoparticles at varying concentration (LFO-Ag 1.5 mmol, LFO-Ag 0.77 mmol, LFO-Ag 0.37 mmol, LFO-Ag 0.19 mmol and LFO-Ag 0.1 mmol) were prepared by spin coating the Ag solutions onto the pre-prepared LFO films to determine the optimum concentration of Ag nanoparticles needed to give the best performance. The PEC performance of the LFO-Ag films were performed in 0.1 M aqueous NaOH (pH 13) solution by illuminating the photocathode from the electrolyte side (represented in schematic 1) to evaluate the current density, compared to plain LFO photocathode. The photocurrent density (J) is plotted against bias potential (V) as shown in Fig. 3. The untreated LFO photocathode exhibited a current density of 0.036 mA/cm^2 at 0.6 V vs RHE. Upon incorporating the 0.77 mmol Ag nanoparticles there is a distinct improvement in the current density reaching 0.061 mA/cm^2 at 0.6 V vs RHE due to the plasmonic enhancement. On increasing the concentration of Ag nanoparticles, slight decrease in current to a value of 0.059 mA/cm^2 as at 0.6 V vs RHE is observed. This will be due to the higher content of Ag nanoparticles on the film surface reducing the electrode/electrolyte interface inhibiting effective charge separation, thus decreasing the amount of current density. As the concentration of the Ag nanoparticles is reduced up to 0.19 mmol, the current density is increased significantly to 0.074 mA/cm^2, an improvement of >2x, compared to the current achieved in a bare $LaFeO_3$ photocathode. At this concentration, a near optimum amount of Ag nanoparticles are incorporated into the film as an optimal current density is achieved, with minimal amount of Ag nanoparticles blocking the electrode/electrolyte interface and achieving the optimum plasmonic effect. Furthermore, dilution to 0.1 mmol sees a drop in current density where it reaches 0.056 mA/cm^2 at 0.6 V vs RHE. As the Ag nanoparticles content decreases further, lower amount of light is trapped for plasmonic resonance, hence there is a drop in current density compared to 0.19 mmol Ag NP concentration. A chronoamperometry test was conducted for the best performing LFO-Ag (0.19 mmol) photocathode to determine its stability. Fig S2 shows the stability of LFO-Ag (0.19 mmol) over a 24 hour period under a continuous 1 sun illumination in 0.1 M NaOH electrolyte solution. The material shows excellent stability over the 24 hour period, reaching a maximum current density of 0.15 mA after 10 hours. At 24 hours there was a slight drop in current density of 5 %. The slight decrease in current density will be due to gas bubble accumulation on the films surface. This will decrease the effective area, increasing the interfacial electrical resistance which causes the slight current drop.[16,45]

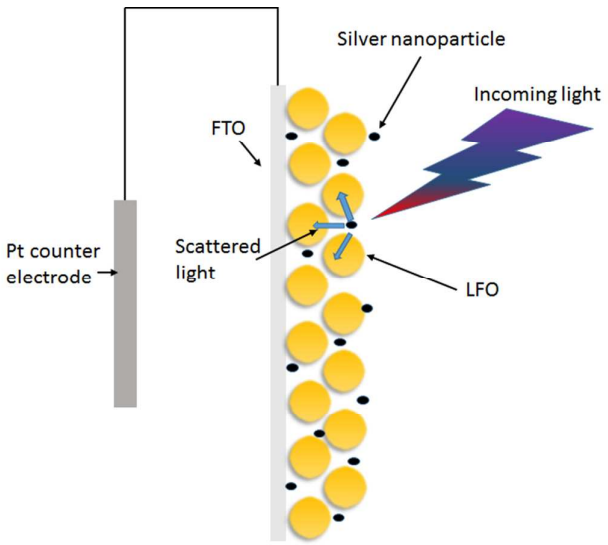

Schematic 1. Image depicting the LFO-Ag working electrode being illuminated where the Ag nanoparticles scatter the light.

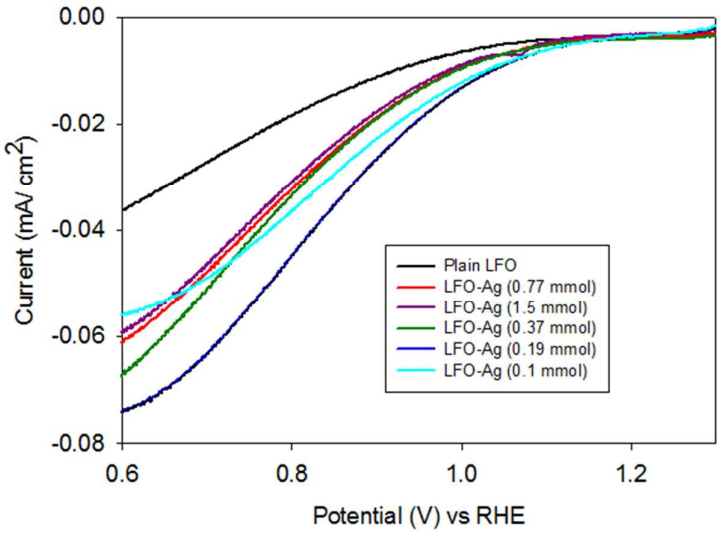

Figure 3. *J-V* characteristics of plain LFO and various LFO-Ag concentrations in a 0.1 M NaOH electrolyte vs RHE.

The best performing LFO-Ag (0.19 mmol) photocathode is used to identify the crystal phase compared to that of plain LFO. The XRD peak pattern for both photocathodes are shown in Fig. 4. The XRD patterns display that the plain LFO films are crystalline with the LFO particles orientated in the (121) plane, which is in good agreement with previous works[16]. All the peaks correspond to LFO are indexed to orthorhombic system (JCPDS 00-037-1493). No Ag diffraction peaks could be clearly identified, which can be attributed to the small particle size, dispersity and low loaded content of Ag nanoparticles. Peaks marked with asterisks correspond to the FTO peaks, distinguishing it from the LFO peaks.

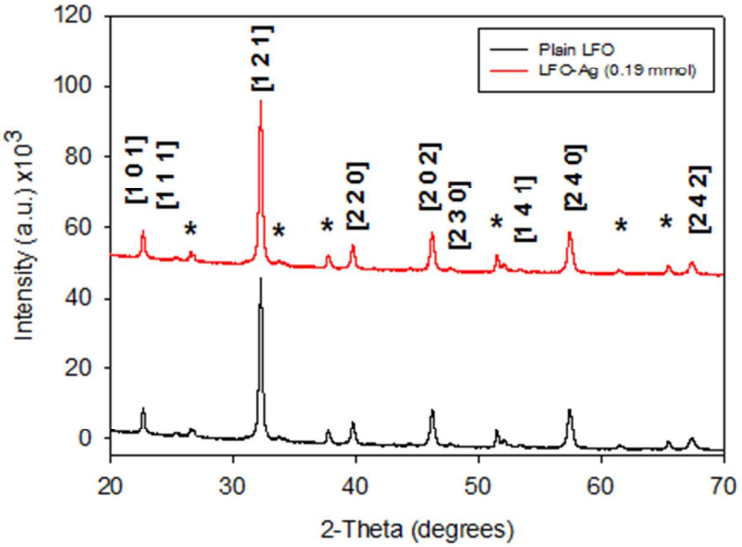

Figure 4. XRD pattern of LFO and LFO-Ag (0.19 mmol) on FTO glass substrate, where the peaks marked with an asterisk represent FTO.

Fig. 5 shows the top view SEM of the plain LFO and LFO-Ag (0.19 mmol). The plain LFO nanostructured film (Fig. 5(a)), and its respective EDS (Fig. 5(c)), have well connected crystal grains in a coral like structure, post annealing 550^{o}C. Its EDS confirms that there is no Ag nanoparticles. Fig. 5(b) shows bright spherical nanoparticles uniformly distributed across the film. These bright spherical can be attributed to the Ag nanoparticles as the EDS (Fig. 5(d)) confirms the presence of Ag. By comparing the two images, it can be clearly seen that the Ag nanoparticles have been incorporated into the LFO film after spin coating.

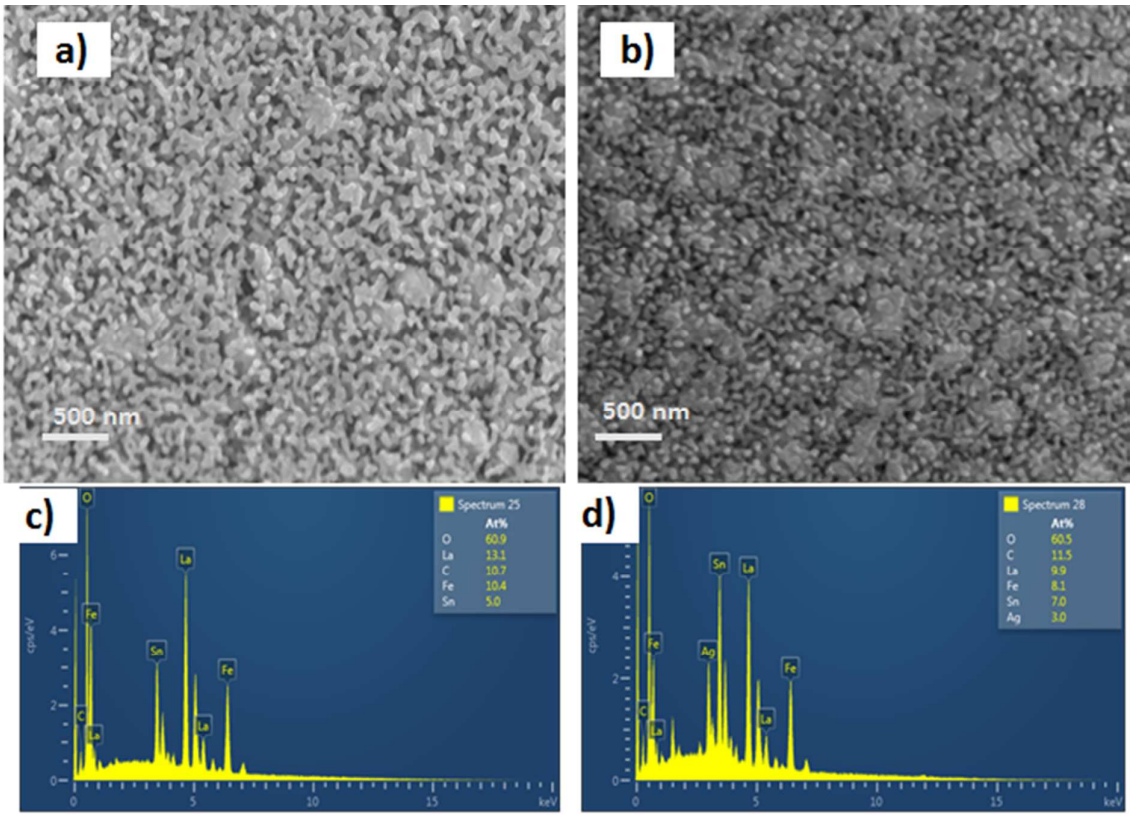

Figure 5. (a) Top view SEM of plain LFO film, **(b)** top view SEM of LFO-Ag (0.19 mmol), **(c)** EDS for plain LFO and **(d)** EDS for LFO-Ag (0.19 mmol).

To understand the effect of Ag nanoparticles on light absorption, its optical properties were measured with UV-Vis spectroscopy. Fig. 6 shows the UV-Vis absorption spectra of both plain LFO and LFO-Ag (0.19 mmol) at wavelengths from 360 – 800 nm. Fig. S2 shows the absorption for all the varying concentrations of LFO-Ag photocathodes. Higher absorption of light in the short wavelength region (400 – 600 nm) and a slight increase in the long wavelength region (600 – 800 nm) was observed for all the LFO-Ag photocathodes, which can be related to the increasing scattering of Ag nanoparticles in this frequency range due to SPR effect. It can be noted that the highest Ag concentration provides the lowest increased absorption of light, where when decreasing the Ag concentration more light is absorbed. This can be because there will be more number of Ag nanoparticles, within a specific area when concentration is highest compared to lower concentration. Therefore, it will reflect some scattered light away from LFO film as Ag is blocking the film due to agglomeration of Ag particles on LFO film surface. When concentration of Ag nanoparticles decreases, the scattered light is directed more towards the LFO film as more of the film is exposed. The optimum concentration for optimum absorbance is 0.19 mmol of Ag nanoparticles. The broad absorption peak observed in the short wavelength region (450 - 500 nm) is due to inhomogeneous size distribution of Ag nanoparticles (50-80 nm) and the peak is slightly blue shifted compared to simulations, which can be due to measurements conducted in air.

The increased absorption shows that the incorporation of Ag nanoparticles effectively enhances the light harvesting when compared to the plain LFO, which is seconded by the

increase in current generated in the case of PEC performance (Fig. 3). Therefore, a higher yield of hydrogen is expected from the solar water splitting experiment as the photocathode potentially absorb more light and generating more current for water splitting.

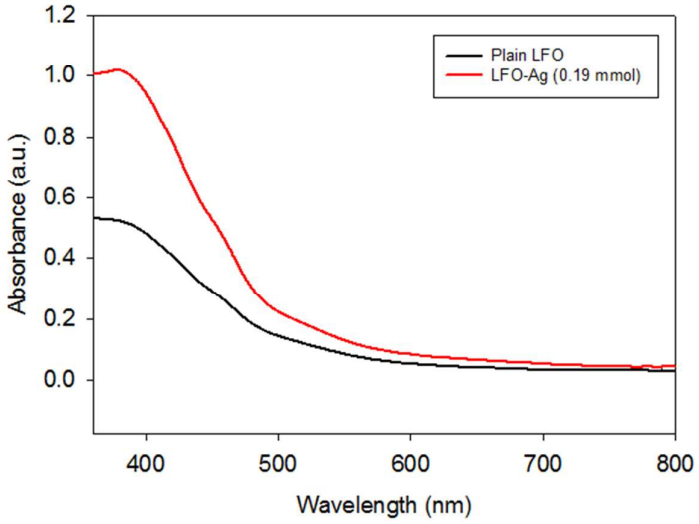

Figure 6. Absorbance spectra of plain LFO and LFO-Ag (0.19 mmol).

Fig. 7 shows the hydrogen evolution measurement of the plain LFO film and LFO films with various Ag NP concentrations performed in an aqueous 0.1 M NaOH solution under a constant illumination. The water splitting test was conducted in a custom made glass reactor vessel with an attached fused silica viewport, described in our previous work.[16] The working electrode and Pt counter electrode were connected by a single looped wire, without any external bias being applied. After 3 hours, the plain LFO photocathode was spontaneously generating hydrogen, where after 6 hours it has generated 0.12 μmol/cm^2. All LFO-Ag photocathodes began spontaneously generating hydrogen after 1 hour. This is a vast improvement compared to the untreated LFO photocathode. This is due to the enhanced light harvesting from the plasmonic effect from the Ag nanoparticles, leading to higher current density being generated, which is in good agreement with the *J-V* curves. As more light is being absorbed by the film, it generates more electrons which are being converted to hydrogen. The hydrogen generated by the different LFO-Ag photocathode concentrations correlates well with the *J-V* curves. As seen in Fig. 3, when decreasing the Ag concentration from 0.77 mmol to 0.19 mmol there is an increase in current. As the current increases there is a clear increase in volume of hydrogen generated; where after 6 hours 0.77 mmol Ag generates 0.21 μmol/cm^2, 0.37 mmol Ag generates 0.22 μmol/ cm^2 and 0.19 mmol Ag generates 0.32 μmol/ cm^2. When the Ag nanoparticles concentration was diluted further to 0.1 mmol the current decreased which also led to a decrease in hydrogen to 0.23 μmol/cm^2. Furthermore, an increase in Ag nanoparticles concentration to 1.5 mmol also led to a decrease in hydrogen generation, where after 6 hours 0.17 μmol/cm^2 of hydrogen is produced. Due to higher content of Ag nanoparticles on the film surface this will reduce the

electrode/electrolyte interface lowering effective charge separation. Furthermore, oxygen evolution also increases simultaneously.

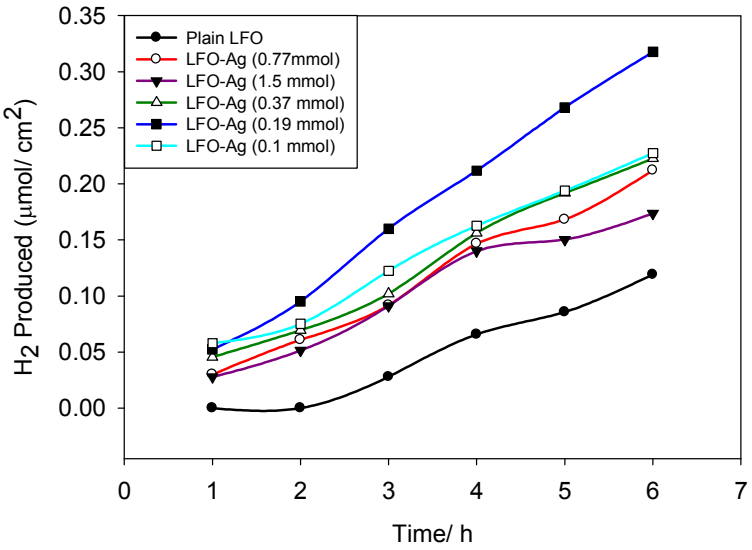

Figure 7. Hydrogen evolution test of plain LFO and LFO-Ag with varying Ag concentrations, in an aqueous 0.1 M NaOH solution.

Conclusion

In summary, we have incorporated optimized Ag nanoparticles (of diameters ranging from 50-80 nm) on to the nanostructured LFO film. The Ag NP shows an enhancement of electric field >7 at the SPR wavelength of 439.5 nm for a diameter of 70 nm. The photocathodes show an increase of light absorption upon incorporation of the Ag nanoparticles compared to its untreated counterpart. This agrees well with the FDTD studies showing better light harvesting for Ag nanoparticles of sizes ranging from 50 nm to 80 nm. Incorporation of Ag nanoparticles has enhanced the current density, where the best performing LFO-Ag (0.19 mmol) photocathode generated twice the amount of current than the plain LFO photocathode generating a current of 0.074 mA/ cm^2 at 0.6 V vs RHE; due to the plasmonic effect from Ag Nanoparticles. Subsequently, the LFO-Ag (0.19 mmol) photocathode generated over twice the amount of hydrogen than the untreated LFO counterpart, where after 6 hours it spontaneously produced 0.32 µmol/cm^2 of hydrogen without the need for an external bias. Furthermore, the LFO-Ag photocathodes were able to produce hydrogen after 1 hour of illumination compared to the untreated LFO photocathode, which began forming hydrogen after 3 hours of illumination. This finding shows that Ag nanoparticles are able to enhance the performance of LFO photocathodes generating a higher volume of hydrogen. Further, studies are required to enhance the performance using nanoparticles of specific diameter and to replace Ag nanoparticles with a lower cost non-precious metal.

Acknowledgement

We acknowledge UKIERI-DST2016-17-0089 project and Engineering and Physical Science Research Council, UK (EPSRC) under the research grant EP/R512801/1 for financial support. A.E. and S.S. would like to thank the Council of Scientific and Industrial Research (CSIR) for the award of Senior Research Fellowship. NSG Pilkington Glass Ltd. is acknowledged for kindly providing the FTO substrates for this work.

Author Information

Corresponding Authors

E-mail: A.Tahir@exeter.ac.uk and balapesala@acsir.res.in

ORCID

Govinder Singh Pawar: 0000-0001-8142-5542

Asif Ali Tahir: 0000-0003-1985-6127

Bala Pesala: 0000-0003-3461-4732

Tapas Kumar Mallick 0000-0002-6456-9955

Notes

The Authors declare no competing financial interest.

Reference

(1) Weisz, P. B. Basic Choices and Constraints on Long-Term Energy Supplies. *Phys. Today* **2004**, *57* (7), 47–52.

(2) Kamat, P. V. Meeting the Clean Energy Demand: Nanostructure Architectures for Solar Energy Conversion. *J. Phys. Chem. C* **2007**, *111* (7), 2834–2860.

(3) Myers, N.; Kent, J. New Consumers: The Influence of Affluence on the Environment. *Proc. Natl. Acad. Sci.* **2003**, *100* (8), 4963–4968.

(4) Xie, G.; Zhang, K.; Guo, B.; Liu, Q.; Fang, L.; Gong, J. R. Graphene-Based Materials for Hydrogen Generation from Light-Driven Water Splitting. *Adv. Mater.* **2013**, *25* (28), 3820–3839.

(5) Holladay, J. D.; Hu, J.; King, D. L.; Wang, Y. An Overview of Hydrogen Production Technologies. *Catal. Today* **2009**, *139* (4), 244–260.

(6) Alfaifi, B. Y.; Ullah, H.; Alfaifi, S.; Tahir, A. A.; Mallick, T. K. Photoelectrochemical Solar Water Splitting: From Basic Principles to Advanced Devices. *Veruscript Funct. Nanomater.* **2018**, 1–26.

(7) Chen, X.; Shen, S.; Guo, L.; Mao, S. S. Semiconductor-Based Photocatalytic Hydrogen Generation. *Therm. Eng.* **2010**, *110*, 6503–6570.

(8) Tachibana, Y.; Vayssieres, L.; Durrant, J. R. Artificial Photosynthesis for Solar Water-Splitting. *Nat. Photonics* **2012**, *6* (8), 511–518.

(9) Osterloh, F. E. Inorganic Nanostructures for Photoelectrochemical and Photocatalytic Water

Splitting. *Chem. Soc. Rev.* **2013**, *42* (6), 2294–2320.

(10) Yang, Y.; Xu, D.; Wu, Q.; Diao, P. Cu2O/CuO Bilayered Composite as a High-Efficiency Photocathode for Photoelectrochemical Hydrogen Evolution Reaction. *Sci. Rep.* **2016**, *6* (1), 35158.

(11) Warren, E. L.; McKone, J. R.; Boettcher, S. W.; Mi…, Q.; Lewis, N. S. Solar Water Splitting Cells. *Chem. Rev.* **2010**, *110*, 6446–6473.

(12) Luo, J.; Steier, L.; Son, M. K.; Schreier, M.; Mayer, M. T.; Gr??tzel, M. Cu2O Nanowire Photocathodes for Efficient and Durable Solar Water Splitting. *Nano Lett.* **2016**, *16* (3), 1848–1857.

(13) Nail, B. A.; Fields, J. M.; Zhao, J.; Wang, J.; Greaney, M. J.; Brutchey, R. L.; Osterloh, F. E. Nickel Oxide Particles Catalyze Photochemical Hydrogen Evolution from Water ; Nanoscaling Promotes P‐Type Character and Minority Carrier Extraction. *ACS Nano* **2015**, *9* (5), 5135–5142.

(14) Ida, S.; Yamada, K.; Matsunaga, T.; Hagiwara, H.; Matsumoto, Y.; Ishihara, T. Preparation of P-Type CaFe2O4 Photocathodes for Producing Hydrogen from Water. *J. Am. Chem. Soc.* **2010**, *132* (49), 17343–17345.

(15) Paracchino, A.; Laporte, V.; Sivula, K.; Grätzel, M.; Thimsen, E. Highly Active Oxide Photocathode for Photoelectrochemical Water Reduction. *Nat. Mater.* **2011**, *10* (6), 456–461.

(16) Pawar, G. S.; Tahir, A. A. Unbiased Spontaneous Solar Fuel Production Using Stable LaFeO3 Photoelectrode. *Sci. Rep.* **2018**, *8* (1), 3501.

(17) Jeong, N. C.; Prasittichai, C.; Hupp, J. T. Photocurrent Enhancement by Surface Plasmon Resonance of Silver Nanoparticles in Highly Porous Dye-Sensitized Solar Cells. *Langmuir* **2011**, *27* (23), 14609–14614.

(18) Lian, Z.; Wang, W.; Xiao, S.; Li, X.; Cui, Y.; Zhang, D.; Li, G.; Li, H. Plasmonic Silver Quantum Dots Coupled with Hierarchical TiO<inf>2</Inf> Nanotube Arrays Photoelectrodes for Efficient Visible-Light Photoelectrocatalytic Hydrogen Evolution. *Sci. Rep.* **2015**, *5* (April), 1–10.

(19) Zhang, Z.; Zhang, L.; Hedhili, M. N.; Zhang, H.; Wang, P. Plasmonic Gold Nanocrystals Coupled with Photonic Crystal Seamlessly on TiO_2 Nanotube Photoelectrodes for Efficient Visible Light Photoelectrochemical Water Splitting. *Nano Lett.* **2013**, *13* (1), 14–20.

(20) Chen, J.-J.; Wu, J. C. S.; Wu, P. C.; Tsai, D. P. Plasmonic Photocatalyst for H 2 Evolution in Photocatalytic Water Splitting. *J. Phys. Chem. C* **2011**, *115* (1), 210–216.

(21) Hu, K.; Chen, H.; Jiang, M.; Teng, F.; Zheng, L.; Fang, X. Broadband Photoresponse Enhancement of a High-Performance t-Se Microtube Photodetector by Plasmonic Metallic Nanoparticles. *Adv. Funct. Mater.* **2016**, *26* (36), 6641–6648.

(22) Chen, H.; Su, L.; Jiang, M.; Fang, X. Highly Desirable Photodetectors Derived from Versatile Plasmonic Nanostructures. *Adv. Funct. Mater.* **2017**, *27* (45), 1–17.

(23) Hu, X.; Xiao, L.; Jian, X.; Zhou, W. Synthesis of Mesoporous Silica-Embedded TiO2 Loaded with Ag Nanoparticles for Photocatalytic Hydrogen Evolution from Water Splitting. *J. Wuhan Univ. Technol. Sci. Ed.* **2017**, *32* (1), 67–75.

(24) Si, Lifang; Qiu, Teng; Zhang, Wenjun; K. Chu, P. Recent Progress in Design of Plasmonic Thin-Film Solar Cells with Enhanced Efficiency. *Recent Patents Mater. Sci.* **2012**, *5* (2), 166–172.

(25) Paul, H.; Fischer, R. How Can a Particle Absorb More than the Light Incident on It? *Am. J.*

Phys. **1983**, *51* (4), 323–327.

(26) Luan, X.; Wang, Y. Plasmon-Enhanced Performance of Dye-Sensitized Solar Cells Based on Electrodeposited Ag Nanoparticles. *J. Mater. Sci. Technol.* **2014**, *30* (1), 1–7.

(27) Wu, N. Plasmonic Metal-Semiconductor Photocatalysts and Photoelectrochemical Cells: A Review. *Nanoscale* **2018**, *10* (6), 2679–2696.

(28) Cushing, S. K.; Wu, N. Progress and Perspectives of Plasmon-Enhanced Solar Energy Conversion. *J. Phys. Chem. Lett.* **2016**, *7* (4), 666–675.

(29) Schaadt, D. M.; Feng, B.; Yu, E. T. Enhanced Semiconductor Optical Absorption via Surface Plasmon Excitation in Metal Nanoparticles. *Appl. Phys. Lett.* **2005**, *86* (6), 1–3.

(30) Stuart, H. R.; Hall, D. G. Island Size Effects in Nanoparticle Enhanced Photodetectors. *Appl Phys Lett* **1998**, *73* (26), 3815–3817.

(31) Pillai, S.; Catchpole, K. R.; Trupke, T.; Green, M. A. Surface Plasmon Enhanced Silicon Solar Cells. *J. Appl. Phys.* **2007**, *101* (9).

(32) Basch, A.; Beck, F. J.; Söderström, T.; Varlamov, S.; Catchpole, K. R. Combined Plasmonic and Dielectric Rear Reflectors for Enhanced Photocurrent in Solar Cells. *Appl. Phys. Lett.* **2012**, *100* (24).

(33) Qi, J.; Dang, X.; Hammond, P. T.; Belcher, A. M. Highly Efficient Plasmon-Enhanced Dye-Sensitized Solar Cells through Metal@oxide Core-Shell Nanostructure. *ACS Nano* **2011**, *5* (9), 7108–7116.

(34) Guo, K.; Li, M.; Fang, X.; Liu, X.; Sebo, B.; Zhu, Y.; Hu, Z.; Zhao, X. Preparation and Enhanced Properties of Dye-Sensitized Solar Cells by Surface Plasmon Resonance of Ag Nanoparticles in Nanocomposite Photoanode. *J. Power Sources* **2013**, *230*, 155–160.

(35) Gangishetty, M. K.; Lee, K. E.; Scott, R. W.; Kelly, T. L. Plasmonic Enhancement of Dye Sensitized Solar Cells in the Red-to-near-Infrared Region Using Triangular Core-Shell Ag@SiO2 Nanoparticles. *ACS Appl Mater Interfaces* **2013**, *5* (21), 11044–11051.

(36) Ihara, M.; Kanno, M.; Inoue, S. Photoabsorption-Enhanced Dye-Sensitized Solar Cell by Using Localized Surface Plasmon of Silver Nanoparticles Modified with Polymer. *Phys. E Low-Dimensional Syst. Nanostructures* **2010**, *42* (10), 2867–2871.

(37) Han, S. C.; Pu, Y. C.; Zheng, L. X.; Hu, L. F.; Zhang, J. Z.; Fang, X. S. Uniform Carbon-Coated CdS Core-Shell Nanostructures: Synthesis, Ultrafast Charge Carrier Dynamics, and Photoelectrochemical Water Splitting. *J. Mater. Chem. A* **2016**, *4* (3), 1078–1086.

(38) Palik, E. D. Handbook of Optical Constants of Solids; 1997.

(39) Hlaing, M.; Gebear-Eigzabher, B.; Roa, A.; Marcano, A.; Radu, D.; Lai, C. Y. Absorption and Scattering Cross-Section Extinction Values of Silver Nanoparticles. *Opt. Mater. (Amst).* **2016**, *58*, 439–444.

(40) Göeken, K. L.; Subramaniam, V.; Gill, R. Enhancing Spectral Shifts of Plasmon-Coupled Noble Metal Nanoparticles for Sensing Applications. *Phys. Chem. Chem. Phys.* **2015**, *17* (1), 422–427.

(41) Fan, X.; Zheng, W.; Singh, D. J. Light Scattering and Surface Plasmons on Small Spherical Particles. *Light Sci. Appl.* **2014**, *3* (March), 1–14.

(42) Steven J. Oldenburg. Silver Nanoparticle Dispersions from Aldrich Materials Science. *Silver Nanoparticles Prop. Appl.* **2014**, No. 730793, 2–5.

(43) Jain, P.; Aggarwal, V. Synthesis, Characterization and Antimicrobial Effects of Silver

Nanoparticles from Microorganisms-A Review. *Int. J. Nano Mater. Sci.* **2012**, *1* (12), 108–120.

(44) Vidhu, V. K.; Philip, D. Catalytic Degradation of Organic Dyes Using Biosynthesized Silver Nanoparticles. *Micron* **2014**, *56*, 54–62.

(45) Hernández, S.; Barbero, G.; Saracco, G.; Alexe-Ionescu, A. L. Considerations on Oxygen Bubble Formation and Evolution on BiVO<inf>4</Inf> Porous Anodes Used in Water Splitting Photoelectrochemical Cells. *J. Phys. Chem. C* **2015**, *119* (18), 9916–9925.

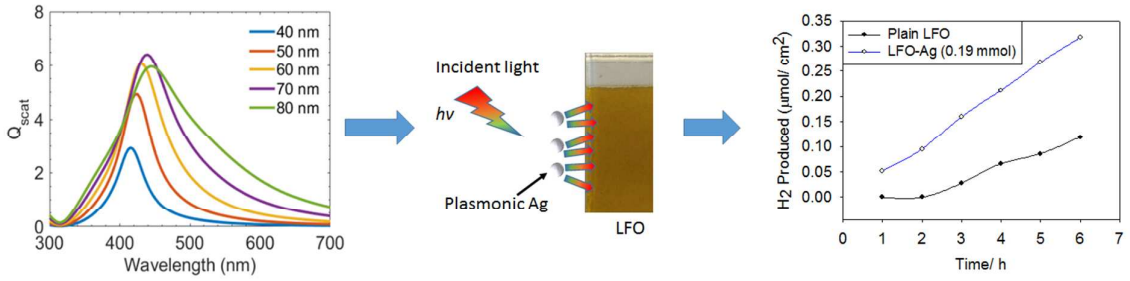

FDTD Simulation

Enhanced Activity

For table of content